Energy-efficient Timetables for Railway Traffic: Incorporating DC Power Models *

Robert Burlacu† Patrick Gemander† Tobias Kuen† Jorge Weston‡

March 11, 2025

Abstract

Efficient operation of underground railway systems is critical not only for maintaining punctual service but also for minimizing energy consumption, a key factor in reducing operational costs and environmental impact. To evaluate the energy consumption of the timetables, this paper delves into the development of mathematical models to accurately represent energy dynamics within the underground railway network.

We evaluate the total traction energy consumption in an underground railway network over a specified period, with the analysis discretized to a per-second basis. At each second we evaluate the power flow in the transmission network, a direct current (DC) power grid with fixed powerstation voltages. Quadratic constraints arise when linking power, current, and voltage. We adjust an existing formulation based on current flows and develop a specialized heuristic for this formulation that enables rapid evaluation of power flows, a critical component for our integrated timetabling approach.

We integrate the model addressing the power flows in the transmission network with the model that ensures the feasibility of the timetable. Central to our approach is the utilization of Benders row generation to tackle the complexity of the large integrated model. By decomposing the optimization problem into manageable subproblems, we enhance computational efficiency and scalability. To linearize the Benders subproblems we develop relaxations for the non-linear constraints and binary variables. We analyze the performance of the integrated timetabling power flow model on real world data provided by the VAG (Verkehrs-Aktiengesellschaft Nürnberg), the operator of public transport in Nuremberg, Germany. The simulated energy consumption deviates from the actual measurements by only around 1%. The calculated timetable increases energy efficiency by up to 0.8% compared to the previously used model. Further numerical studies demonstrate the effectiveness of the developed solving algorithms.

1 Introduction

The underground railway system is a widely used urban transportation network recognized for its effectiveness and, along with trams, as one of the cleanest forms of public transport, see Moreno et al., 2015. The study of energy efficiency in underground railway systems has gained relevance in light of growing global concerns about climate change and the need for clean energy solutions. A critical area of research is reducing energy consumption within DC networks, which represent one of the highest operational costs for underground railway systems. This work specifically focuses on reducing energy consumption in an underground railway system through efficient scheduling and the recovery of braking energy from trains.

*This work was part of the Project EKSSE, funded by the Bundesministerium für Bildung und Forschung (BMBF).

†Fraunhofer-Institut für Integrierte Schaltungen IIS, Gruppe Optimization, Nordostpark 84, 90411 Nürnberg, Germany, (robert.burlacu@iis.fraunhofer.de, patrick.gemander@fau.de, tobias.kuen@iis.fraunhofer.de).

‡Friedrich-Alexander-Universität Erlangen-Nürnberg, Chair Data Science, Cauerstraße 11, 91058 Erlangen, Germany, jorge.weston@fau.de

Adjusting timetables can significantly impact energy consumption in underground railway systems. Two key factors are relevant in this context: First, the optimal utilization of braking energy, and second, the extension of coasting phases. By synchronizing the braking and accelerating phases of trains, it is possible to capture and reuse braking energy effectively, thereby reducing the overall energy consumption. Additionally, longer running times allow for extended coasting phases, further decreasing energy consumption for individual trains.

However, the efficiency gains from capturing braking energy are tempered by inherent losses in the transmission network, particularly when trains are far apart. The transmission network in underground railway systems operates on a DC power grid, presenting unique challenges for mathematical modeling. Proper optimization techniques are essential for accurately representing the complex dynamics of DC power flows and timetabling.

Energy recovery can be approached in two ways: first, using storage devices to store energy generated during braking, which can then be used to accelerate trains when needed (known as wayside storage); and second, by synchronizing accelerating and braking trains to properly coordinate the energy supplied by braking trains and reduce the amount of energy required from the power network.

Several studies have addressed energy efficiency in underground railway systems through various approaches. For example, Gao and L. Yang, 2019; H. Liu et al., 2018; P. Liu et al., 2018; Su et al., 2013; X. Yang et al., 2015; Zhao et al., 2017 consider the timetable problem alongside train speed profiles to find energy-efficient timetables, but they often overlook the characteristics of DC networks and the related transmission energy losses. These studies focus mainly on the kinetic energy recovery problem and differ in timetable constraints and solution approaches, such as brute force algorithms and various metaheuristics. Similarly, P. Liu et al., 2018 included storage devices in the timetabling with speed profiles model. In S. Yang et al., 2020, the timetabling with speed profiles model is solved alongside a passenger assignment problem via bi-objective optimization using a metaheuristic, later extended in Huang, Liao, and Gao, 2021 to multiple interconnected lines. Finally, Gupta, Van Parys, and Tobin, 2023 present a timetabling with energy recovery, where the energy is approximated via a data-driven approach.

However, these works often do not adequately consider the transmission losses in a DC power network, assuming they can be neglected due to the distance between trains. This assumption can lead to issues. For example, with low-frequency timetables where the distance between trains is greater, the energy recovered from braking might not be sufficient to meet the energy required by accelerating trains. In their study to minimize the energy consumption of a DC railway system via voltage control on substations, Raghunathan et al., 2014 provide a model to represent the transmission losses accurately. Hager and Kuen, 2024 adjust this model to optimize the voltages at the power stations at the underground network in Nuremberg, Germany.

Also for timetabling, a joint approach of timetabling and a model that accounts for power grid losses is essential to prevent overestimating recovered energy and to ensure proper network operation.

Comprehensive reviews of timetabling and energy efficiency in railway systems can be found in Scheepmaker, Goverde, and Kroon, 2017. Arboleya et al., 2020 provide a review of railway feeding infrastructures, and Kang et al., 2024 offer an up-to-date review of underground train timetabling and rescheduling problems.

This work builds upon a successful energy optimization project with VAG, the operator of the underground train system in Nuremberg. In Bärmann et al., 2021, the authors demonstrated a theoretical potential for energy savings of up to 8.5% through optimized timetabling. The model has since been successfully implemented at VAG, where real-world measurements show actual energy savings between 2% and 3%. While this might seem modest, it translates to significant cost savings. For instance, considering the Frankfurt metro system's annual energy consumption of approximately 120 GWh , see Verkehrsgesellschaft Frankfurt am Main (VGF), 2022, a 3% reduction would result in savings of 3,600 MWh per year. At current European industrial electricity prices Eurostat, 2024, this translates into annual cost savings of around €712,000. In addition, considering that underground railway systems typically operate for decades, these incremental improvements contribute to substantial long-term environmental and economic benefits without requiring infrastructure

modifications. One key factor contributing to the gap between theoretical 8.5% and actual 2-3% savings is the current simplification in modeling power networks, where power losses on transmission lines are neglected.

This paper aims to address this limitation by developing a more accurate model that accounts for these losses. Our model integrates the synchronization of braking and accelerating trains with the power flow dynamics in a DC network, resulting in a non-convex mixed-integer quadratically constrained problem. To address the non-convexity, we develop a heuristic that, through linear approximation and relaxation, converges to a solution that satisfies the physical dynamics of the problem. Our algorithm ensures that the timetabling solutions we propose are both energy-efficient and practical for real-world implementation.

The contributions of this paper are twofold. First, we use an accurate model for DC power flow in underground railway networks that captures transmission losses and physical constraints stated in Hager and Kuen, 2024. Instead of optimizing the power station voltages, we consider those as fixed and use the model purely as a simulation tool. We develop a heuristic to solve this simulation model fast. Second, we integrate this power flow model into timetable optimization, developing efficient solution methods including a Benders decomposition approach and linearization techniques. This integration allows us to simultaneously optimize train schedules while accurately accounting for energy dynamics, leading to more realistic and efficient solutions.

The key to making this integrated approach computationally tractable is the newly introduced efficient heuristic for solving the DC power flow model. While we employ a standard Benders decomposition framework, the challenge lies in handling the non-convex power flow subproblems that must be solved repeatedly. Our main technical contribution is developing careful convexification techniques and a specialized heuristic that makes these subproblems tractable. The heuristic achieves this by linearizing the non-convex power flow constraints while maintaining high solution quality, as demonstrated by its deviation of only around 1% from real-world measurements.

The remainder of this paper is structured as follows. Section 2 presents the energy-related problem for a fixed timetable. We introduce and compare the current flow problem with the power flow problem in a fixed timetable, introduce the heuristic, and analyze its computational performance. In Section 3, we present the integrated model, considering timetabling and physical dynamics, along with the different solving strategies. Section 4 presents our computational study, and finally, in Section 5, we conclude and suggest possible extensions.

2 Simulation Model for a Fixed Timetable

In this section we focus on the physical model of the electricity flow for a fixed train configuration at a particular moment, i.e., the power flow in the railway network for a given timetable. First, we start by describing in a general way the network that will be considered, and later we present the mathematical formulation based on Current Flow (CF). The model is a non-convex quadratic continuous model. Moreover, given the power station gates in our network it is necessary to include new binary variables and constraints, making the formulation mixed-integer non-convex, which is known to be NP-hard in general. Therefore, we develop a heuristic based on a linearization of the model that can tackle this problem in an efficient way and allows us to later integrate timetable planning with the power flow simulation.

2.1 Modeling Assumptions

To understand how the DC railway power system works, we first discuss its fundamental principles. In a DC railway network, power stations provide electrical energy to trains through overhead lines or a third rail system. The power flow in such a system is bidirectional - trains can both consume and generate power. When a train accelerates or climbs a grade, it consumes power, while modern trains can generate power through regenerative braking, where the train's motors act as generators, converting kinetic energy back into electrical energy. This regenerated power can be used by other trains in the network, leading to significant energy savings.

We model the network as a directed graph, where each power line has a designated source and destination node. The current flow direction in a power line is represented by the sign of the current value: positive current indicates flow from source to destination, while negative current indicates flow from destination to source. For most power lines, current can flow in either direction, except for the connections between power station sources and power stations, where current can only flow from source to station.

The voltage level in the network plays a crucial role in system efficiency and safety. Power stations maintain a constant voltage level, but the voltage at other points in the network can vary. These variations occur due to power consumption and transmission losses. If the voltage drops too low, trains may not receive sufficient power for operation. Conversely, if voltages become too high, it could damage equipment. Therefore, maintaining appropriate voltage levels throughout the network is essential for safe and efficient operation.

Our model of this DC power system is built on several key assumptions. The network operates purely on direct current, with power station source nodes maintaining constant, equal voltage levels. While source voltages are fixed, the voltages at other nodes - including power stations, accelerating trains, and braking trains - can vary within specified operational bounds. Power can only flow from power station sources to power stations, not in reverse, which we implement through gate constraints.

The physical network is represented as a graph where power stations and trains form the nodes, and power lines form the arcs. Train positions are discretized according to their location in the network. The network topology follows a straight line configuration, where train nodes have two adjacent nodes, while power stations have three adjacent nodes due to their connection to a power station source node.

Power demands and supplies in the network are known for each train position and time. Accelerating trains have fixed positive power demands, while braking trains can supply power back to the network through regenerative braking. The model accounts for power losses in transmission lines using standard DC power flow equations based on voltage differences and line admittances, ensuring accurate representation of the energy flow in the system.

2.2 Power Network

Let us represent the dynamic network by a graph G_t for t in the time horizon T, and let $A(G_t)$ and $V(G_t)$ be the set of arcs and set of nodes of the graph, respectively. The set $V(G_t)$ is partitioned into:

- Power stations and power station sources, represented by $V^{PS}(G)$ and $V^{PSS}(G)$, respectively. These nodes do not change over time.
- Braking trains and accelerating trains: The trains position, and behavior, changes over time. These nodes will be denoted by $V^{BT}(G_t)$ and $V^{AT}(G_t)$, respectively. Each train node $u \in V^{BT}(G_t) \cup V^{AT}(G_t)$ has an associated power demand p_u, where $p_u > 0$ for accelerating trains ($u \in V^{AT}(G_t)$) and $p_u < 0$ for braking trains ($u \in V^{BT}(G_t)$).

Finally, let us define by $A^{PS}(G)$ the arcs connecting the power stations with their respective source, this set represent the only time-independent arcs of the graph. Figure 1 represents an example network for a given time. Here, we have 2 accelerating trains depicted in violet and one braking train in yellow driving between 3 stations. The powerstation source nodes are colored orange, the power station nodes teal. In what follows we will omit the time dependency and focus on the network for a particular time, in Section 3 the time dependency will be again considered. Each node $u \in V(G)$, following Watt's law, is characterized by power P_u, current I_u, and voltage U_u. For the particular case of the power station sources, the voltage is a fixed quantity that is known beforehand and will be denoted by $\mathcal{U}$. We also assume that all the power station sources have equal fixed voltages. The power flows along the arcs of the network, for a particular arc $(u, v) \in A(G)$ this can be represented as current flow I_{uv}, or as power flow, going out of node u towards node v, P_{uv}^{from} and arriving at node v from node u, P_{uv}^{to}.

The power flows from higher to lower voltage. However, when the voltage of the power station is higher than the voltage of its respective source a power flow will translate into energy inefficiency for our network. Therefore, to avoid this situation there are gates that only allow power to flow from power station sources to power stations and prevent flow in the

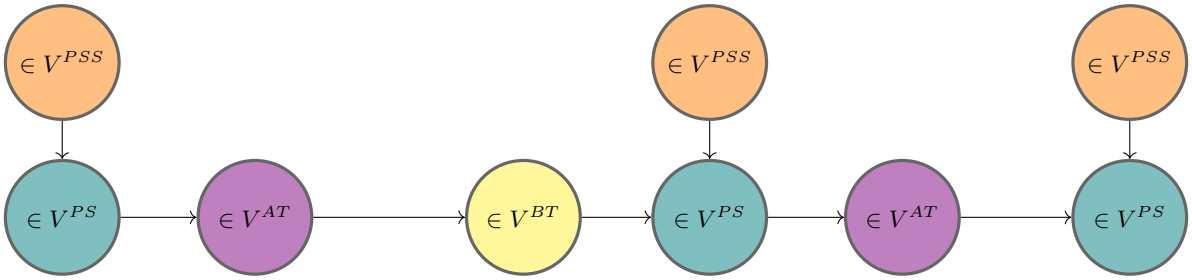

Figure 1: Transmission graph G.

opposite direction. From a modeling point of view, this is achieved by incorporating a binary variable δ_{uv} for all power station arcs $(u, v) \in A^{PS}(G)$ that will activate the arc only if the voltage of the power station source is higher than the voltage in the power station. Finally, the losses along each arc $(u, v) \in A(G)$ are represented with an admittance parameter c_{uv}. The value of this parameter depends on the length of the power line and its material, so we can break it down further to

$$c_{uv} = \frac{\omega}{d_{uv}},$$

where ω is the material constant of the power line and d_{uv} represents its physical length.

2.3 Current Flow Model CF

Following closely the formulation presented by Hager and Kuen, 2024, and taking into consideration the specific characteristics of our network, the current flow model can be written as:

$$\min_{I,U,\delta} \sum_{(u,v)\in A^{PS}(G)} I_{uv} \tag{CF.1}$$

$$\text{s.t. } I_v = \sum_{w\in\delta^{\text{out}}(v)} I_{vw} - \sum_{u\in\delta^{\text{in}}(v)} I_{uv}, \qquad v \in V^{BT} \cup V^{AT}(G), \tag{CF.2}$$

$$0 = \sum_{w\in\delta^{\text{out}}(v)} I_{vw} - \sum_{u\in\delta^{\text{in}}(v)} I_{uv}, \qquad v \in V^{PS}(G), \tag{CF.3}$$

$$U_u \cdot I_u \leq -p_u, \qquad u \in V^{BT} \cup V^{AT}(G), \tag{CF.4}$$

$$I_{uv} = c_{uv}(U_u - U_v), \qquad (u, v) \in A(G) \setminus A^{PS}(G), \tag{CF.5}$$

$$I_{uv} \geq c_{uv}(\mathcal{U} - U_v), \qquad (u, v) \in A^{PS}(G), \tag{CF.6}$$

$$I_{uv} - M\delta_{uv} \leq c_{uv}(\mathcal{U} - U_v), \qquad (u, v) \in A^{PS}(G), \tag{CF.7}$$

$$I_{uv} \leq M(1 - \delta_{uv}), \qquad (u, v) \in A^{PS}(G), \tag{CF.8}$$

$$\mathcal{U} - U_v \leq M(1 - \delta_{uv}), \qquad (u, v) \in A^{PS}(G), \tag{CF.9}$$

$$I_{uv} \geq 0, \qquad (u, v) \in A^{PS}(G), \tag{CF.10}$$

$$\underline{U}_u \leq U_u \leq \overline{U}_u, \qquad u \in V(G) \setminus V^{PSS}(G), \tag{CF.11}$$

$$\delta \in \{0, 1\}. \tag{CF.12}$$

In here, the objective (CF.1) is to minimize the current injected into the network by the power station sources. Constraints (CF.2) and (CF.3) represent the current flow conservation, i.e., Kirchhoff's first law, for the trains and the power stations, respectively. (CF.4) model the demand (supply) of the accelerating (braking) trains. Ohm's law, for the arcs that are not connected to a power station source, is modeled with constraints (CF.5). Since we do not allow for flow back into the powerstation source nodes, the current flow on the power station arcs is positive (CF.10). The voltages at all nodes are bounded from above and below (CF.11). Finally, constraints (CF.6)-(CF.9) model the activation of the arcs connecting the power stations with their respective source. If these gate variables are set to one, Ohm's law is neglected at the associated arc (CF.7), (CF.6), no flow is permitted on

the arc (CF.8) and the voltage on the power station node has to be lower than the fixed voltage at the power source node (CF.9).

Model (CF) is computationally challenging due to two factors: the non-convex quadratic constraints (CF.4) linking voltage, current, and power demand, and the binary variables required for modeling the power station gates in constraints (CF.8)-(CF.9). This model serves as the basis for evaluating the energy consumption of the timetables. Comparisons between the traction current data measured and simulated by the VAG (Verkehrs-Aktiengesellschaft Nürnberg), the operator of public transport in Nuremberg, Germany show that the deviation is only around 1%.

2.4 Current Model Linearization

The only non-linearity in Model (CF) is in constraints (CF.4). However, we can approximate these constraints by replacing in these inequalities the voltage variable U_u with a constant value Y_u. Particularly, if $Y_u = \overline{U}_u$ for braking trains and $Y_u = \underline{U}_u$ for accelerating trains we obtain an inner approximation of the problem. With this, we can obtain the following mixed-integer linear problem as an inner approximation of Model (CF)

$$\min_{I,U,\delta} \sum_{u \in V^{PS}(G)} \sum_{v \in \delta^{\text{out}}(u)} I_{uv} \tag{LCF.1}$$

$$\text{s.t. } I_u = \sum_{v \in \delta^{\text{out}}(u)} I_{uv} - \sum_{v \in \delta^{\text{in}}(u)} I_{vu}, \qquad u \in V^{BT} \cup V^{AT}(G), \tag{LCF.2}$$

$$0 = \sum_{v \in \delta^{\text{out}}(u)} I_{uv} - \sum_{v \in \delta^{\text{in}}(u)} I_{vu}, \qquad u \in V^{PS}(G), \tag{LCF.3}$$

$$I_u \leq \frac{-p_u}{Y_u}, \qquad u \in V^{BT} \cup V^{AT}(G), \tag{LCF.4}$$

$$I_{uv} = c_{uv}(U_u - U_v), \qquad (u,v) \in A(G) \setminus A^{PS}(G), \tag{LCF.5}$$

$$I_{uv} \geq c_{uv}(\mathcal{U} - U_v), \qquad (u,v) \in A^{PS}(G), \tag{LCF.6}$$

$$I_{uv} - M\delta_{uv} \leq c_{uv}(\mathcal{U} - U_v), \qquad (u,v) \in A^{PS}(G), \tag{LCF.7}$$

$$I_{uv} \leq M(1 - \delta_{uv}), \qquad (u,v) \in A^{PS}(G), \tag{LCF.8}$$

$$\mathcal{U} - U_v \leq M(1 - \delta_{uv}), \qquad (u,v) \in A^{PS}(G), \tag{LCF.9}$$

$$I_{uv} \geq 0, \qquad (u,v) \in A^{PS}(G), \tag{LCF.10}$$

$$\underline{U}_u \leq U_u \leq \overline{U}_u, \qquad u \in V(G) \setminus V^{PSS}(G), \tag{LCF.11}$$

$$\delta \in \{0,1\}. \tag{LCF.12}$$

Model (LCF) overestimates the real current demand on accelerating trains and underestimates the current supply on braking trains.

2.5 Linear Current Model Heuristic HEU

Even if the linearization used to obtain Model (LCF) is naive and not tight, we can make use of an iterative procedure to improve the approximated constraints and converge to a solution that is feasible for Model (CF). Now, we introduce a heuristic that makes the current demands and supplies approach their actual values, and we also present some remarks regarding the convergence of the heuristic.

As it was previously stated, Model (LCF) is an inner approximation of Model (CF). The heuristic gradually adapts the demand constraints (LCF.4) towards the optimal solution of Model (CF). The heuristic starts by using the voltage's bounds, i.e., $Y_u = \overline{U}_u$ for braking trains and $Y_u = \underline{U}_u$ for accelerating trains. Then, we can optimize Model (LCF) and use the solution to update the values of Y_u. This procedure is repeated until the change in Y is smaller than a tolerance ϵ. The heuristic is summarized in Algorithm 1, where $\tilde{I}$ is the optimal solution to Model (CF).

Assuming we can use all the available current from braking trains, and that all accelerating trains use exactly the current they demand, we can calculate the solution for Model (LCF) efficiently in $\mathcal{O}(|A(G)|)$. The solution quality of the heuristic compared to

Algorithm 1: Linear Current Model Heuristic HEU

Data: Graph G, Parameters c, p, $\underline{U}$, $\overline{U}$, $\epsilon > 0$
Result: Current flow $I^* \approx \tilde{I}$

$Y_u \leftarrow \underline{U}_u, \quad u \in V^{AT}(G)$;
$Y_u \leftarrow \overline{U}_u, \quad u \in V^{BT}(G)$;
Solve Model LCF;
while $\|U^* - Y\|_2 > \epsilon$ **do**
  $Y_u \leftarrow U^*_u, \quad u \in V^{BT} \cup V^{AT}(G)$;
  Solve Model LCF

solving Model (CF) directly is controlled by the parameter ϵ. The choice of ϵ represents a trade-off between solution accuracy and computational speed. A smaller ϵ leads to solutions closer to the optimal solution of Model (CF), but requires more iterations of the algorithm. Specifically, since the voltage updates in each iteration become smaller as we approach the optimal solution (as shown in the convergence proof below), a very small ϵ may require many additional iterations to achieve only marginal improvements in solution quality. In our computational experiments, we found that $\epsilon = 10^{-5}$ provides a good balance, typically requiring only 6-7 iterations while achieving solutions that deviate by less than 0.1% from the optimal solution of Model (CF).

Remark 2.1. *For given values for δ_{uv} and I_{uv} $\forall (u,v) \in A^{PS}(G)$ and I_u $\forall u \in V^{BT} \cup V^{AT}(G)$ one can calculate all currents and voltages in the network G in $\mathcal{O}(|A(G)|)$, if a solution to Model* (CF) *exists.*

To better represent the order of the nodes, we introduce an alternative notation for the nodes in G, see Figure 2. The colors of the nodes are chosen as in Figure 1. When considering only power stations and trains (ignoring power station sources), the network forms a linear structure. The power stations are enumerated from 1 to n, where power station k is adjacent to power station $k-1$ and power station $k+1$ for all $k \in 2, ..., n-1$. For each $k \in [n]$ the corresponding power station source node is named k, the power station node is named k_0. The trains on a path between two neighboring power station nodes k_0 and $(k+1)_0$ get enumerated from 1 to m_k, where m_k is the number of trains between the two power station nodes. The corresponding train node is named k_l for $l \in [m_k]$ and $k \in [n]$. The line distance between 2 not necessarily adjacent nodes u and v is denoted by $d_{u,v}$ In Figure 2, we show the voltage values U_{k_l} at each node k_l, where U_{k_l} represents the voltage variable associated with node k_l. For all $k \in [n-1]$, we can calculate the voltage of a train node $k_{l'}$ from its

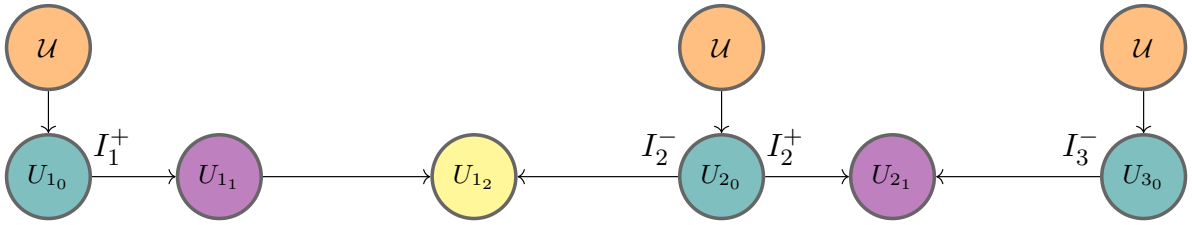

Figure 2: Ordered transmission graph G.

left-next and from its right-next power station node

$$U_{k_0} - \frac{d_{k_0,k_{l'}}}{\omega} I_k^+ - \sum_{l=1}^{l'-1} \frac{d_{k_l,k_{l'}}}{\omega} I_{k_l} = U_{k_{l'}} =$$
$$U_{(k+1)_0} - \frac{d_{k_{l'},(k+1)_0}}{\omega} (-\sum_{l=1}^{m_k} I_{k_l} - I_k^+) - \sum_{l=l'+1}^{m_k} \frac{d_{k_{l'},k_l}}{\omega} I_{k_l}.$$

This equation is derived from the fact that the voltage $U_{k_{l'}}$ at train node $k_{l'}$ can be calculated in two equivalent ways:

From the left power station k_0:

- Starting with voltage U_{k_0} at power station k_0
- Subtracting voltage drop $\frac{d_{k_0,k_{l'}}}{\omega} I_k^+$ due to current I_k^+ flowing from station k_0 to train $k_{l'}$
- Subtracting voltage drops $\sum_{l=1}^{l'-1} \frac{d_{k_l,k_{l'}}}{\omega} I_{k_l}$ due to currents of all trains between station k_0 and train $k_{l'}$

From the right power station $(k+1)_0$:

- Starting with voltage $U_{(k+1)_0}$ at power station $(k+1)_0$
- Subtracting voltage drop $\frac{d_{k_{l'},(k+1)_0}}{\omega}(-\sum_{l=1}^{m_k} I_{k_l} - I_k^+)$ due to total current flowing from train $k_{l'}$ to station $(k+1)_0$
- Subtracting voltage drops $\sum_{l=l'+1}^{m_k} \frac{d_{k_{l'},k_l}}{\omega} I_{k_l}$ due to currents of all trains between train $k_{l'}$ and station $(k+1)_0$

This allows us to obtain the value for I_k^+ for all $k \in [n-1]$ depending on the voltages at the nearest power station nodes

$$I_k^+ = -\sum_{l=1}^{m_k} \frac{d_{k_l,(k+1)_0}}{d_{k_0,(k+1)_0}} I_{k_l} + \frac{\omega}{d_{k_0,(k+1)_0}}(U_{k_0} - U_{(k+1)_0}). \tag{1a}$$

If we consider only two power station sources, this reduces to

$$I_1^+ = -\sum_{l=1}^{m_1} \frac{d_{1_l,2}}{d_{1,2}} I_{1_l}. \tag{1b}$$

since the current from the power station source node equals the current from the power station node. Assume $n \geq 3$. Ohm's law at each power station arc yields

$$\begin{aligned}
U_{1_0} &= \mathcal{U} - \frac{d_{1,1_0}}{\omega} I_1^+, \\
U_{k_0} &= \mathcal{U} - \frac{d_{k,k_0}}{\omega}(-\sum_{l=1}^{m_{k-1}} I_{(k-1)_l} - I_{k-1}^+ + I_k^+), \quad \forall k \in \{2,...,n-1\}, \\
U_{n_0} &= \mathcal{U} - \frac{d_{n,n_0}}{\omega}(-\sum_{l=1}^{m_{n-1}} I_{(n-1)_l} - I_{n-1}^+).
\end{aligned} \tag{1c}$$

Define

$$\begin{aligned}
a_k &\coloneqq d_{k,k+1}, && \forall k \in [n-1], \\
b_k &\coloneqq -d_{k,k_0}, && \forall k \in [n-1], \\
r_1 &\coloneqq -\sum_{l=1}^{m_1} d_{1_l,2} I_{1_l}, \\
r_k &\coloneqq -\sum_{l=1}^{m_k} d_{k_l,k+1} I_{k_l} + \sum_{l=1}^{m_{k-1}} d_{k,k_0} I_{(k-1)_l}, && \forall k \in \{2,...,n-1\}.
\end{aligned}$$

Combining (1a) and (1c) establishes a relationship between the current flows from power station sources given by the following equation system:

$$\underbrace{\begin{pmatrix} a_1 & b_2 & 0 & \cdots & 0 \\ b_2 & a_2 & b_3 & \ddots & \vdots \\ 0 & b_3 & a_3 & \ddots & 0 \\ \vdots & \ddots & \ddots & \ddots & b_{n-1} \\ 0 & \cdots & 0 & b_{n-1} & a_{n-1} \end{pmatrix}}_{\mathcal{A}} \underbrace{\begin{pmatrix} I_1^+ \\ I_2^+ \\ \vdots \\ I_{n-2}^+ \\ I_{n-1}^+ \end{pmatrix}}_{I^+} = \underbrace{\begin{pmatrix} r_1 \\ r_2 \\ \vdots \\ r_{n-2} \\ r_{n-1} \end{pmatrix}}_{r}. \tag{2}$$

Being a tridiagonal matrix with non-zero entries on the diagonals, $\mathcal{A}$ is invertible and we can calculate I^+ using Thomas algorithm Thomas, 1949 in $\mathcal{O}(n)$. I_k^- is then given by the equations

$$I_k^- = -\sum_{l=1}^{m_{k-1}} I_{(k-1)_l} - I_{k-1}^+ \quad \forall k \in \{2, ..., n\}$$

and arc currents by Kirchhoff's first law. Lastly, $U_{k_{l'}}$ for $k \in [n-1]$, $l' \in [m_k]$ can be calculated as

$$U_{k_{l'}} = \mathcal{U} - \frac{d_{k,k_0}}{\omega}(I_k^- + I_k^+) - \sum_{l=1}^{l'} \frac{d_{l-1,l}}{\omega} I_k^+ - \sum_{l=1}^{l'-1} \frac{d_{l,l+1}}{\omega} I_{k_l}.$$

The complexity of $\mathcal{O}(|A(G)|)$ follows from the calculation steps: For $n \geq 3$ power stations, computing I^+ requires solving the tridiagonal system using Thomas algorithm in $O(n)$ operations. Then computing I_k^- for each $k \in \{2, ..., n\}$ requires summing over m_{k-1} train currents, and finally computing train voltages requires one calculation per train node. Since the number of arcs $|A(G)|$ is proportional to the number of power stations plus the total number of trains ($\sum_{k=1}^{n-1} m_k$), all calculations can be performed in $O(|A(G)|)$ operations.

Remark 2.2. *If the network only consists of two power stations and accelerating trains, Algorithm 1 converges to the optimal solution of Model* (CF)*, if it exists.*

We use the notation of Remark 2.1. The voltage at each accelerating train node $U_{1_{l'}}$ for all $l \in [m_k]$ can be calculated as follows. From (1b), we already know the current coming from power station 1.

$$I_1^+ = -\sum_{l=1}^{m_1} \frac{d_{1_l,2}}{d_{1,2}} I_{1_l}. \tag{3a}$$

Now we can obtain the voltage at the accelerating train $1_{l'}$.

$$U_{1_{l'}} = \mathcal{U} + \frac{d_{1,1_{l'}}}{\omega} \sum_{l=1}^{m_1} \frac{d_{1_l,2}}{d_{1,2}} I_{1_l} - \sum_{l=1}^{l'-1} \frac{d_{1,1_{l'}} d_{1_l,2}}{\omega d_{1,2}} I_{1_l}. \tag{3b}$$

To proof that Algorithm 1 converges, we show that the voltage at each train node increases monotonously. Being bounded from above, this sequence converges, which implies $U_{1_l}^{i+1} - U_{1_l}^i \to 0$.

$$\begin{aligned} U_{1_{l'}}^{i+1} - U_{1_{l'}}^i = &- \frac{d_{1,1_{l'}}}{\omega} \sum_{l=l'}^{m_1} \underbrace{\frac{d_{1_l,2}}{d_{1,2}}}_{>0} p_{1_l} \left(\frac{1}{U_{1_l}^i} - \frac{1}{U_{1_l}^{i-1}}\right) \\ &- \sum_{l=1}^{l'-1} \underbrace{\frac{d_{1,1_{l'}} d_{1_l,2} - d_{1_l,1_{l'}} d_{1,2}}{\omega d_{1,2}}}_{= \frac{d_{1,l} d_{l',2}}{\omega d_{1,2}} > 0} p_{1_l} \left(\frac{1}{U_{1_l}^i} - \frac{1}{U_{1_l}^{i-1}}\right). \end{aligned}$$

The statement follows by induction and the fact that all voltages increase in the first iteration because they were initialy set to their lower bound. All solution voltages in each iteration lie between their lower bound and the optimal solution of Model (CF) and are therefore feasible.

The algorithm converges to $U_{1_l}^{i+1} - U_{1_l}^i \to 0$ and thus towards a solution $(\tilde{U}, \tilde{I})$ that satisfies $\tilde{U}_{1_l} \tilde{I}_{1_l} = -p_{1_l}$ for all train nodes $l \in [m_1]$. This is now a feasible solution for Model (CF) for which all demand constraints are tight. The only way to improve this solution would be by increasing the currents at the train nodes further without increasing the value for $I_{1_l} U_{1_l}$. Using previous transformations, we have for all $l' \in [m_1]$

$$I_{1_{l'}} U_{1_{l'}} = I_{1_{l'}} \left(\mathcal{U} - \frac{d_{1,1_{l'}}}{\omega} \sum_{l=l'}^{m_1} \frac{d_{1_l,2}}{d_{1,2}} I_{1_{l'}} - \sum_{l=1}^{l'-1} \frac{d_{1,l} d_{l',2}}{\omega d_{1,2}} I_{1_{l'}}\right).$$

Taking the derivative of this function with respect to $I_{1_{l'}}$ yields

$$\begin{aligned}\frac{\partial I_{1_{l'}} U_{1_{l'}}}{\partial I_{1_{l'}}} &= \mathcal{U} - \frac{d_{1,1_{l'}}}{\omega} \sum_{l=l'}^{m_1} \frac{d_{1_l,2}}{d_{1,2}} I_{1_l} - \sum_{l=1}^{l'-1} \frac{d_{1,l} d_{l',2}}{\omega d_{1,2}} I_{1_l} - \frac{d_{1,1_{l'}}}{\omega} \frac{d_{1_l,2}}{d_{1,2}} I_{1_{l'}} \\ &= U_{1_{l'}} - \frac{d_{1,1_{l'}}}{\omega} \frac{d_{1_l,2}}{d_{1,2}} I_{1_{l'}},\end{aligned}$$

which is greater than zero. Hence, increasing the current at a train node comes with increasing the power at the node and there is no better solution to Model (CF) than $(\tilde{U}, \tilde{I})$ found by Algorithm 1.

In Table 1 we compare the runtime of solving Model (CF) to the runtime of the developed heuristic (HEU). The performance tests were implemented in Python 3.10.13 using Gurobi 11.0.0 with standard parameter setting to solve mixed-integer quadratic problems. We performed the calculations on a laptop with an Intel i7-1165G7 CPU, 32 GB RAM, 4 cores and 2.80 GHz base frequency. The stated runtimes are average times over all instances of one configuration in seconds. The configurations are named

$$(|V^{PS}(G)|, |V^{AT}(G)|, |V^{BT}(G)|, \max_{u \in V^{BT} \cup V^{AT}(G)} |p_u|).$$

The column $ITER$ represents the average number of steps in the heuristic, so the number of linear models we have to solve to get to an ϵ value of $1e^{-5}$. Note that on average we only have to solve 6 linear models to obtain a close approximation to the optimal solution to the non-linear Model (CF). This, together with the fact that we can utilize a warmstart for the linear models in each steps, yields a significant speedup of 87% in the runtime on average.

Table 1: Runtime test solving Model CF with Gurobi compared to the runtime of Algorithm 1 and number of steps in the heuristic.

Instance	ITER	CF	HEU
(10, 5, 5, 2)	3.3	0.048	0.009
(25, 10, 10, 2)	3.9	0.197	0.020
(50, 25, 25, 2)	4.1	4.322	0.045
(100, 50, 50, 2)	4.5	11.365	0.102
(10, 5, 5, 10)	6.7	0.045	0.017
(25, 10, 10, 10)	7.2	0.137	0.034
(50, 25, 25, 10)	9.7	2.081	0.109
(100, 50, 50, 10)	10.3	6.375	0.245
Average	6.2	3.071	0.072

The efficiency of this heuristic is one of the main building blocks for our overall solution approach. For the later integration of the power flow model with timetable optimization using Benders decomposition, we need to repeatedly solve power flow subproblems - one for each time period and each candidate timetable. Without a fast method for solving these subproblems, the Benders approach would be computationally intractable. Our heuristic makes this integration possible by providing quick yet accurate power flow solutions.

3 Embedding into Timetabling Model

We now aim to integrate the developed model for the DC power network with the underground train timetable optimization model. By shifting departure times and lengthening running times we can improve both the driving behaviour of the trains and the usage of braking energy in the system to reduce the total energy consumption.

3.1 Modeling a Feasible Timetable

The modeling of a feasible timetable is taken from Gemander, Bärmann, and Martin, 2023. Binary variables x_{kij} are introduced which in the case $x_{kij} = 1$ indicate that the train on leg k departs at time i with running time j. A leg is defined as a train's direct movement from one station to its immediately adjacent station. The tuple (k, i, j) is called a departure configuration. For each leg k we have to choose exactly one departure configuration. Besides these multiple-choice constraints, the timetable also has to satisfy constraints regarding headway times, dwell times and turnaround times. This implies that that the choice of some configurations is mutually exclusive. The set of X contains all binary solution vectors x representing a feasible timetable. The way how X is defined is explained in detail in Gemander, Bärmann, and Martin, 2023. Each departure configuration has a power profile assigned to it. This specifies the power demand of (k, i, j) in each second $i, i + 1, ..., i + j$. For each $t \in [i, i + j]$ the power demand of the train with departure configuration (k, i, j) is known and given as p_{kijt}. Knowing the departure time, running time and power profile we can also state the location of the train with departure configuration (k, i, j) at time $t \in [i, i + j]$.

3.2 Transmission Graph Adjustment

The transmission graph introduced in Section 2 for fixed timetables contains nodes representing trains at specific locations. When integrating timetable optimization, we need to adapt this graph structure to handle multiple possible train positions and departure times while maintaining the same physical network properties.

For each timestamp $t \in T$, we group departure configurations (k, i, j) that demand power at time t into buckets. A bucket $B(u)$ represents a set of departure configurations that are active at time t, are located in approximately the same position l along their respective legs, and have similar power demands. More precisely, a departure configuration (k, i, j) is active at time t if $t \in [i, i + j]$, meaning the train is running during that timestamp.

The buckets are constructed such that any two departure configurations within the same bucket are mutually exclusive in a feasible timetable. This mutual exclusivity occurs either because the configurations belong to the same leg (as only one departure time and running time can be chosen per leg), or because safety regulations (like minimum headway times) prevent two trains from occupying the same track section simultaneously.

Each bucket is assigned to a node u in the transmission graph, replacing what would be a single train node in the fixed timetable model. The potential power demand of bucket node u is defined as the mean power demand of the departure configurations inside the bucket: $p_u = \frac{\sum_{(kij) \in B(u)} p_{kijt}}{|B(u)|}$. This creates a crucial connection between the timetabling and power flow models: Once the timetable variables x_{kij} are fixed, each bucket node effectively becomes equivalent to a train node in the fixed timetable model. Specifically:

- If exactly one departure configuration in bucket u is selected ($x_{kij} = 1$), the bucket node behaves like a train node with the fixed power demand p_u.

- If no departure configuration in the bucket is selected (all $x_{kij} = 0$), the bucket node acts as a train node with zero power demand, which our model can handle naturally through the power flow equations.

This power demand p_u is activated if and only if one of the assigned departure configurations is selected in the timetable solution.

We term the maximum proximity between two departure configurations in one bucket the *resolution* of the transmission graph, where the proximity of two departure configurations (k_1, i_1, j_1) and (k_2, i_2, j_2) is defined as

$$\left\| \begin{pmatrix} \frac{t-i_1}{2j_1} \\ p_{k_1 i_1 j_1 t} \end{pmatrix} - \begin{pmatrix} \frac{t-i_2}{2j_2} \\ p_{k_2 i_2 j_2 t} \end{pmatrix} \right\|_2$$

for all $t \in T$.

The first component of each vector represents the relative position of the train along its leg at time t, normalized to $[0, 1]$ where 0 indicates the start of the leg and 1 the end. The second component is the power demand at time t. Thus, the formula measures how similar two departure configurations are in terms of both their spatial location and power consumption. Configurations with similar positions and power demands will be grouped into the same bucket.

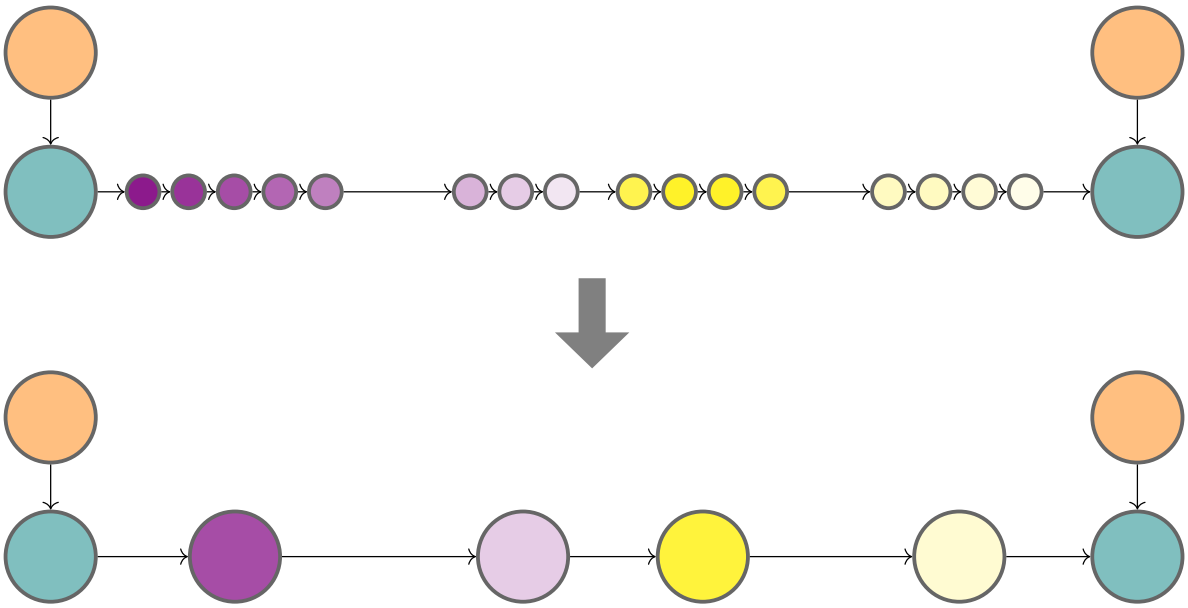

Figure 3: Grouping departure configuration nodes into buckets for transmission graph G_t with timetabling.

Instead of train nodes, the transmission network now contains bucket nodes located at the center of the departure configurations it contains, as shown in Figure 3. The power stations and their source nodes remain unchanged from the fixed timetable model, maintaining the same physical network structure. This adaptation allows us to model the power flow for all possible timetable configurations while preserving the electrical properties of the network.

This prevents large admittance parameters causing numerical issues which would arise if two departure configurations are located too close to each other.

3.3 Admittance Adjustment

When a timetable has been selected, many bucket nodes will have power demand zero, since none of the assigned departure configurations has been chosen. The addition of nodes with zero power demand into the network should have no impact to the overall flow. To archieve this we have to properly determine the admittance parameters. In an example of three nodes where node 2 has zero power demand, we can state the following relationship between the voltages.

$$(U_1 - U_2)c_{12} = (U_2 - U_3)c_{23}$$
$$\Rightarrow U_2 = \frac{U_1 c_{12} + U_3 c_{23}}{c_{12} + c_{23}}.$$

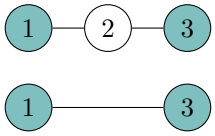

The current should be equal for all arcs $(1,2)$, $(2,3)$ and $(1,3)$. Therefore the admittance parameter when deleting node 2 can be calculated as

$$(U_1 - U_3)c_{13} = (U_1 - U_2)c_{12}$$
$$\Rightarrow c_{13} = \frac{c_{12}c_{23}}{c_{12} + c_{23}}. \tag{4}$$

As we define the admittance on an arc as a constant ω over the length d of the power line the arc represents. This fulfills (4) since

$$d_{uw} = d_{uv} + d_{vw} \quad \Rightarrow \quad \frac{\omega}{d_{uw}} = \frac{\frac{\omega}{d_{uv}}\frac{\omega}{d_{vw}}}{\frac{\omega}{d_{uv}} + \frac{\omega}{d_{vw}}}$$

holds for all $\omega, d_{uw}, d_{uv}, d_{vw} \in \mathbb{R}^+$.

3.4 Timetabling Model BASE

The mixed integer timetabling model stated in Gemander, Bärmann, and Martin, 2023 seeks to minimize the positive part of the sum of all power demands at one timestamp t for all $t \in T$

$$\min_{z,x} \sum_{t \in T} z_t \tag{BASE.1}$$
$$\text{s.t.} \sum_{u \in V^{BT} \cup V^{AT}(G_t)} \sum_{(k,i,j) \in B(u)} p_{kijt} x_{kij} \leq z_t, \qquad t \in T, \tag{BASE.2}$$
$$z \geq 0 \tag{BASE.3}$$
$$x \in X. \tag{BASE.4}$$

The z-variables can be interpreted as the amount of power that is requested from the powerstations, assuming there is no limit on the voltages in the network and no transmission loss on the lines. This model underestimates the actual power demand of the grid and serves as a base model for the study in this paper.

3.5 Integrated Timetabling Current Flow Model CM

The goal is to integrate the constraints implied by physical laws into the (BASE) model. To archieve this, we use Model CF as the evaluation function for the timetables.

$$\min_{I,U,\delta,x} \sum_{t\in T} \sum_{(u,v)\in A^{PS}(G_t)} I_{uv} \tag{CM.1}$$

$$\text{s.t. } I_u = \sum_{v\in\delta^{\text{out}}(u)} I_{uv} - \sum_{v\in\delta^{\text{in}}(u)} I_{vu}, \qquad u \in V^B(G_t),\ t \in T, \tag{CM.2}$$

$$0 = \sum_{v\in\delta^{\text{out}}(u)} I_{uv} - \sum_{v\in\delta^{\text{in}}(u)} I_{vu}, \qquad u \in V^{PS}(G_t),\ t \in T, \tag{CM.3}$$

$$U_u \cdot I_u \leq \sum_{(k,i,j)\in B(u)} -p_{kijt} x_{kij}, \qquad u \in V^B(G_t),\ t \in T, \tag{CM.4}$$

$$I_{uv} = c_{uv}(U_u - U_v), \qquad (u,v) \in A(G_t) \setminus A^{PS}(G_t),\ t \in T, \tag{CM.5}$$

$$I_{uv} \geq c_{uv}(\mathcal{U} - U_v), \qquad (u,v) \in A^{PS}(G_t),\ t \in T, \tag{CM.6}$$

$$I_{uv} - M\delta_{uv} \leq c_{uv}(\mathcal{U} - U_v), \qquad (u,v) \in A^{PS}(G_t),\ t \in T, \tag{CM.7}$$

$$I_{uv} \leq M(1-\delta_{uv}), \qquad (u,v) \in A^{PS}(G_t),\ t \in T, \tag{CM.8}$$

$$\mathcal{U} - U_v \leq M(1-\delta_{uv}), \qquad (u,v) \in A^{PS}(G_t),\ t \in T \tag{CM.9}$$

$$I_{uv} \geq 0, \qquad (u,v) \in A^{PS}(G_t),\ t \in T, \tag{CM.10}$$

$$\underline{U}_u \leq U_u \leq \overline{U}_u, \qquad u \in V(G_t) \setminus V^{PSS}(G_t),\ t \in T, \tag{CM.11}$$

$$\delta \in \{0,1\}, \tag{CM.12}$$

$$x \in X. \tag{CM.13}$$

The coupling of the models takes place in the Constraints (CM.4). For each $t \in T$, the demand at each bucket node $u \in V^B(G_t)$ is given by the power demand p_{kijt} of the active departure configuration x_{kij} inside the bucket. The buckets are defined such that there is at most one departure configuration active inside it. Fixing the x variables and therefore commiting to one timetable leads exactly to Model CF which was shown to be solvable efficiently in Section 2.5.

3.6 Solving Strategies

Model CM is a mixed-integer nonlinear problem and is therefore computationally very hard to solve as a whole. Our solution approach greatly benefits from the fast heuristic developed in Section 2.5, which allows us to efficiently evaluate power flows in the Benders decomposition subproblems. This section provides different strategies, relaxations and algorithms that build on this heuristic to deal with the overall problem complexity. First, we try to relax the parts of the model, that make it hard to solve, namely the binary part in the gate constraints (CM.8), (CM.9) and the quadratic terms in (CM.4).

3.6.1 Relaxing Gate Constraints

For each $t \in T$, the gate constraints (CM.6), (CM.7), (CM.8), (CM.9) and (CM.12) can be relaxed to

$$I_{uv} \geq c_{uv}(\mathcal{U} - U_v), \quad (u,v) \in A^{PS}(G_t), \tag{RG.1}$$

$$I_{uv} \leq c_{uv}(\overline{U}_v - U_v)\frac{\mathcal{U} - \underline{U}_v}{\overline{U}_v - \underline{U}_v}, \quad (u,v) \in A^{PS}(G_t) \tag{RG.2}$$

$$\sum_{u\in V^{BT}\cup V^{AT}(G_t)} \sum_{(k,i,j)\in B(u)} p_{kijt}\tilde{x}_{kij} \leq \sum_{(u,v)\in A^{PS}(G_t)} \mathcal{U} I_{uv}. \tag{RG.3}$$

The blue line in Figure 4 depicts the feasible set defined by (CM.6), (CM.7), (CM.8) and (CM.9). Inequality (RG.1) yields an overestimator for the current shown by the red line in Figure 4. The relaxation allows for some amount of current to flow from a power

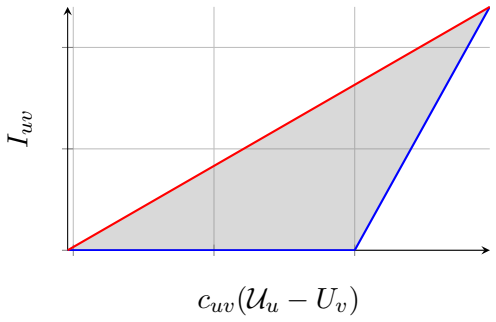

Figure 4: Gate constraint relaxation.

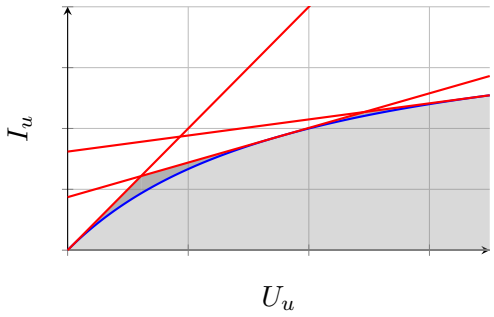

Figure 5: Feasibility set for U_u and I_u with relaxation of demand constraints at accelerating buckets, assuming $P_u = -p_u$.

station source node u to a power station node v although there is a higher voltage on v than on u. In special cases, this could even lead to a higher voltage at the power station source node than at an accelerating train. To prevent the case in which less power is supplied than demanded, we introduce constraints (RG.3).

3.6.2 Relaxing Quadratic Power Balance Constraints

When relaxing the quadratic demand constraints (CM.4) it is helpful to differentiate between buckets that only contain departure configurations with positive power demand, so called accelerating buckets $V^{AB}(G_t)$ and braking buckets $V^{BB}(G_t)$, which only contain configurations with negative power demand. For accelerating buckets, the constraint $U_u \cdot I_u \leq -p_u$ with $p_u > 0$ defines a convex set, as it represents the area below a hyperbola in the first quadrant. For braking buckets, where $p_u < 0$, the same constraint defines a concave set, as it represents the area above a hyperbola. This geometric difference requires different relaxation strategies for the two types of buckets, as shown in Figures 5 and 6.

Accelerating Trains The power flowing into a node $u \in V^{AB}(G_t)$ in an optimal solution only takes two possible values. If one of the departure configurations inside the bucket $(i,k,j) \in B(u)$ is selected the value is $-p_{kijt}$, 0 otherwise. We introduce a variable for the power flowing into node u, P_u. For each $t \in T$ for a chosen value $\underline{U}_u \leq \mathcal{V}_u \leq \overline{U}_u$ we introduce a cut to relax (CM.4) that tangents $I_u = \frac{P_u}{U_u}$ at $P_u = -p_u$ and $U_u = \mathcal{V}_u$. Numerical experiments show, that the three support points $\mathcal{V} \in \mathcal{S}_u := \{\underline{U}_u, \frac{\underline{U}_u + \overline{U}_u}{2}, \overline{U}_u\}$, as depicted in Figure 5 are adequate.

$$I_u \leq \frac{p_u}{\mathcal{V}^2} U_u + \left(\frac{-\underline{U}_u}{\mathcal{V}^2} + \frac{2}{\mathcal{V}}\right) P_u - p_u \frac{\underline{U}_u}{\mathcal{V}^2}, \quad u \in V^{AB}(G_t),\ \mathcal{V} \in \mathcal{S}_u, \tag{AD.1}$$

$$I_u \leq 0, \quad u \in V^{AB}(G_t), \tag{AD.2}$$

$$P_u \leq \sum_{(k,i,j) \in B(u)} -p_u x_{kij}, \quad u \in V^{AB}(G_t). \tag{AD.3}$$

Constraint (AD.1) is chosen to not cut of the point $I_u = P_u = 0$. This point should be feasible and is enforced by constraints (AD.3) and (AD.2) if no departure configuration is active in the bucket.

Braking Trains To relax the quadratic constraints for each $t \in T$ (CM.4) for braking trains we use

$$I_u \leq \frac{p_u}{\underline{U}_u \overline{U}_u} U_u - p_u \left(\frac{1}{\underline{U}_u} + \frac{1}{\overline{U}_u}\right), \quad u \in V^{BB}(G_t), \tag{BD.1}$$

$$I_u \cdot \underline{U}_u \leq \sum_{(k,i,j) \in B(u)} -p_u x_{kij}, \quad u \in V^{BB}(G_t). \tag{BD.2}$$

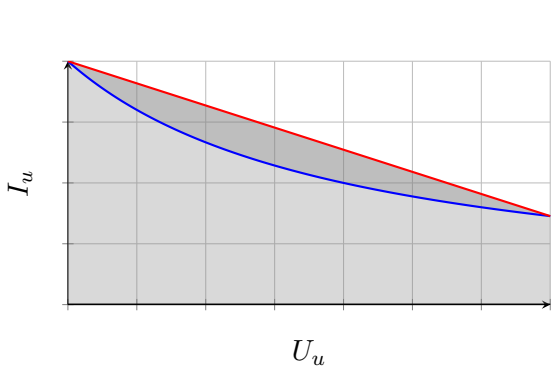

(a) Relaxation without using piecewise linearization

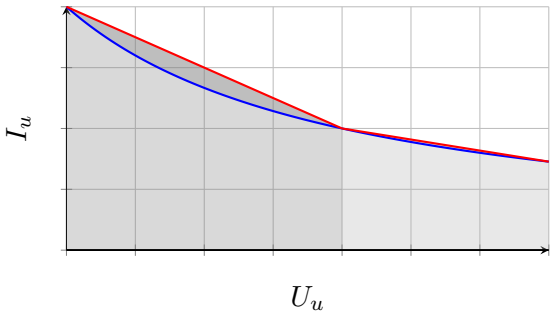

(b) Relaxation using piecewise linearization

Figure 6: Feasibility set for U_u and I_u with relaxation of demand constraints at braking buckets.

Zero or negative current flow if no departure configuration in the bucket is active is enforced by constraints (BD.2). We can increase the tightness of the relaxation using the concept of piecewise linearization. For each breaking train node $u \in V^{BB}(G_t)$ we add a binary variable γ_u indicating whether $U_u \leq \mathcal{V}_u$ or $U_u \geq \mathcal{V}_u$ holds for a chosen support point $\mathcal{V}$. When relaxing quadratic power balance constraints piecewise linear we replace constraints (BD.1) by

$$I_u \leq \frac{p_u}{\underline{U}_u \mathcal{V}} U_u - p_u\left(\frac{1}{\underline{U}_u} + \frac{1}{\mathcal{V}_u}\right) + M\gamma_u, \quad u \in V^{BB}(G_t), \tag{RP.1}$$

$$I_u \leq \frac{p_u}{\mathcal{V}\overline{U}_u} U_u - p_u\left(\frac{1}{\mathcal{V}_u} + \frac{1}{\overline{U}_u}\right) + M(1-\gamma_u), \quad u \in V^{BB}(G_t), \tag{RP.2}$$

$$U_u \leq \mathcal{V}_u + M\gamma_u, \quad u \in V^{BB}(G_t), \tag{RP.3}$$

$$U_u \geq \mathcal{V}_u + M(1-\gamma_u), \quad u \in V^{BB}(G_t), \tag{RP.4}$$

for a chosen value $\underline{U}_u \leq \mathcal{V}_u \leq \overline{U}_u$. The feasible sets for (BD.1) or (RP), respectively, is depicted in Figure 6.

The fully relaxed version of Model CM with constraints (RG),(AD) and (BD), we term RLX. The most accurate linearization of Model CM using only the relaxed constraints (RP) is termed SB.

3.6.3 Adaptive piecewise linearization

In many optimization problems, adaptive refinement of piecewise linear relaxations can improve performance by adding more support points only where needed. However, this approach is not effective for our power flow problem. The reason lies in the network structure: power can flow through multiple paths between any two points, and the solver will always choose the path with the loosest approximation to artificially reduce the objective value. For example, if we refine the approximation for one braking bucket but leave another coarser, the solver will route more power through the less accurately approximated bucket to exploit the larger approximation error there. Therefore, we must maintain uniform approximation accuracy across all buckets to prevent such exploitation of the relaxation.

3.6.4 Benders Cut Generation

While the structure of Model CM naturally suggests a Benders decomposition approach, the non-convex nature of the power flow subproblems presents a significant challenge. Our key contribution is making this standard decomposition technique work effectively through:

- Careful convexification of the subproblems using the relaxations developed in Sections RG-RP
- Application of our specialized heuristic from Section 2.5 to solve the resulting subproblems quickly and accurately

The decomposition divides the problem into a master problem for timetable selection (Model BASE) and power flow evaluation subproblems for each timestep. The fast solution of these subproblems through our heuristic is crucial, as they must be solved repeatedly during the Benders iteration process.

The subproblems are the relaxed versions of Model CM with fixed timetable variables $\tilde{x}, \tilde{z}$, including relaxations (RG), (AD) and (BD).

Benders Subproblem for $t \in T$

$$\min_{I,U} \sum_{(u,v)\in A^{PS}(G_t)} I_{uv} \tag{BS.1}$$

$$\text{s.t. } -\tilde{z}_t \leq - \sum_{(u,v)\in A^{PS}(G_t)} I_{uv}, \qquad (\alpha^1) \tag{BS.2}$$

$$0 = -I_u + \sum_{v\in\delta^{\text{out}}(u)} I_{uv} - \sum_{v\in\delta^{\text{in}}(u)} I_{vu}, \qquad u \in V^B(G_t), \tag{BS.3}$$

$$0 = \sum_{v\in\delta^{\text{out}}(u)} I_{uv} - \sum_{v\in\delta^{\text{in}}(u)} I_{vu}, \qquad u \in V^{PS}(G_t), \tag{BS.4}$$

$$p_u\left(\frac{1}{\underline{U}_u} + \frac{1}{\overline{U}_u}\right) \leq \frac{p_u}{\underline{U}_u \overline{U}_u} U_u - I_u, \qquad u \in V^{BB}(G_t), \qquad (\alpha^2_u) \tag{BS.5}$$

$$\sum_{(k,i,j)\in B(u)} p_{kijt}\tilde{x}_{kij} \leq -I_u \cdot \underline{U}_u, \qquad u \in V^{BB}(G_t), \qquad (\alpha^3_u) \tag{BS.6}$$

$$p_u \frac{\underline{U}_u}{\mathcal{V}^2} \leq \frac{p_u}{\mathcal{V}^2} U_u + \left(\frac{-\underline{U}_u}{\mathcal{V}^2} + \frac{2}{\mathcal{V}}\right) P_u - I_u, \qquad u \in V^{AB}(G_t),\ \mathcal{V} \in \mathcal{S}_u, \qquad (\alpha^4_u\mathcal{V}) \tag{BS.7}$$

$$0 \leq -I_u, \qquad u \in V^{AB}(G_t), \tag{BS.8}$$

$$\sum_{(k,i,j)\in B(u)} p_{kijt}\tilde{x}_{kij} \leq -P_u, \qquad u \in V^{AB}(G_t), \qquad (\alpha^5_u) \tag{BS.9}$$

$$c_{uv}\mathcal{U} \leq I_{uv} + c_{uv}U_v, \qquad (u,v) \in A^{PS}(G_t), \qquad (\alpha^6_{uv}) \tag{BS.10}$$

$$-c_{uv}\overline{U}_v \frac{\mathcal{U} - \underline{U}_v}{\overline{U}_v - \underline{U}_v} \leq -I_{uv} - c_{uv}U_v \frac{\mathcal{U} - \underline{U}_v}{\overline{U}_v - \underline{U}_v}, \qquad (u,v) \in A^{PS}(G_t), \qquad (\alpha^7_{uv}) \tag{BS.11}$$

$$\sum_{u\in V^{BT}\cup V^{AT}(G_t)} \sum_{(k,i,j)\in B(u)} p_{kijt}\tilde{x}_{kij} \leq \sum_{(u,v)\in A^{PS}(G_t)} \mathcal{U} I_{uv}, \qquad (\alpha^8) \tag{BS.12}$$

$$0 = -I_{uv} + c_{uv}(U_u - U_v), \qquad (u,v) \in A(G_t) \setminus A^{PS}(G_t), \tag{BS.13}$$

$$0 \leq I_{uv}, \qquad (u,v) \in A^{PS}(G_t), \tag{BS.14}$$

$$\underline{U}_u \leq U_u, \qquad u \in V(G_t), \qquad (\alpha^9_u) \tag{BS.15}$$

$$-\overline{U}_u \leq -U_u, \qquad u \in V(G_t). \qquad (\alpha^{10}_u) \tag{BS.16}$$

Additionaly, (BS.7) connects the variables representing the total energy consumption at time t, z_t from Model BASE with the total consumption calculated in the subproblem. As long as the total consumption is underestimated by Model BASE, the respective subproblem will be infeasible. For an extreme ray $\tilde{\alpha}$ of the dual of

Model 11, we can introduce the following feasibility cut for each $t \in T$

$$
\begin{aligned}
0 \leq & -\tilde{\alpha}^1 z_t \\
& + \sum_{u \in V^{BB}(G_t)} \tilde{\alpha}^2_u p_u \left(\frac{1}{\underline{U}_u} + \frac{1}{\overline{U}_u}\right) \\
& + \sum_{u \in V^{BB}(G_t)} \tilde{\alpha}^3_u \sum_{(k,i,j) \in B(u)} p_{kijt} x_{kij} \\
& + \sum_{u \in V^{AB}(G_t)} \sum_{\mathcal{V} \in \mathcal{S}_u} \tilde{\alpha}^4_{u\mathcal{V}} p_u \frac{\underline{U}_u}{\mathcal{V}^2} \\
& + \sum_{u \in V^{AB}(G_t)} \tilde{\alpha}^5_u \sum_{(k,i,j) \in B(u)} p_{kijt} x_{kij} \\
& + \sum_{(u,v) \in A^{PS}(G_t)} \tilde{\alpha}^6_{uv} c_{uv} \mathcal{U} \\
& + \sum_{(u,v) \in A^{PS}(G_t)} -\tilde{\alpha}^7_{uv} c_{uv} \overline{U}_v \frac{\mathcal{U} - \underline{U}_v}{\overline{U}_v - \underline{U}_v} \\
& + \tilde{\alpha}^8 \sum_{u \in V^{BT} \cup V^{AT}(G_t)} \sum_{(k,i,j) \in B(u)} p_{kijt} x_{kij} \\
& + \sum_{u \in V(G_t)} \tilde{\alpha}^9_u \underline{U}_u \\
& + \sum_{u \in V(G_t)} -\tilde{\alpha}^{10}_u \overline{U}_u
\end{aligned}
$$

to Model BASE. This cut can be interpreted as a lower bound on the total power consumption at time t, represented by z_t in Model BASE when selecting timetable x. Note that we only generate feasibility cuts and no optimality cuts in our Benders approach. This is because the objective value of the master problem (z_t) already represents the total power consumption at time t. The subproblem's role is solely to verify whether this power consumption is physically achievable given the network constraints. If the subproblem is infeasible, it means the master problem has underestimated the required power, and we add a feasibility cut to correct this underestimation. If the subproblem is feasible, the master problem's objective value already correctly represents the true power consumption, making optimality cuts unnecessary.

Implementation of Benders Decomposition We implemented and tested the presented Benders approach in two ways. Whenever we added the cuts from the subproblems in one iteration, we can chosoe to solve the resulting master problem to optimality or we can generate the cuts using a callback function at each node in the branch-and-bound tree of the master problem. Both approaches have their own advantages. When solving the master problem to optimality in each iteration, we at the same time obtain a lower bound for the integrated model. Using the callback method, the master problem does not have to be solved to optimality in each iteration, therefore the cuts can be added more efficiently. The disadvantage of this method is a slow improvement of the lower bound for the integrated model. We term BCB the callback approach. BS represents solving the master problem to optimality in each iteration.

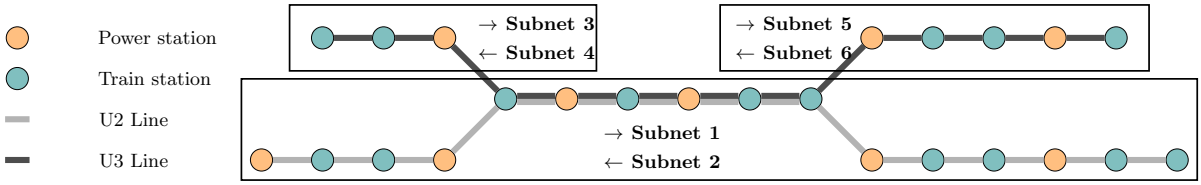

Figure 7: Underground train network map in Nuremberg.

4 Computational Results

In this section, we present the computational results for the models developed and solving strategies to optimize the timetables of the underground train network considering the power flows. All algorithms were implemented in Python 3.10.13 using Gurobi 11.0.0 with standard parameter setting to solve mixed-integer problems. We performed the calculations on a server with an Intel Xeon Gold 6326 CPU, 256 GB RAM, 2x16 cores, and 2.9 GHz base frequency. The Gurobi solver was limited to 8 threads to avoid memory issues.

4.1 Test Instances

All tests were performed on real-world deployed timetables provided by our project partners VAG, the operator of the underground train system in Nuremberg, Germany. We consider two different timetables, one for weekdays and one for sundays. They differ in frequency of the schedule, there drive fewer trains per hour on sundays than on weekdays. To make the timetable optimization applicable in real operations, we use a rolling horizon approach where we optimize segments of the timetable throughout the day. This allows us to react to real-time disruptions and delays by adjusting upcoming segments, keep computation times manageable by focusing on shorter time windows while maintaining solution quality by considering segments long enough to capture relevant train interactions.

For our computational experiments, we therefore analyze segments of the timetable between 100 and 700 seconds, which is sufficient to evaluate the model's performance while maintaining practical relevance.

The transmission network for the DC power simulation is also designed to match the real state of the underground train system in Nuremberg, including information about the track lengths and admittance parameters on the power lines. The section we are looking at consists of 6 separate subgrids with a total of 24 substations. The subnets are divided into three regions, with the two directions of travel separated, as depicted in Figure 7.

4.2 Resolution Sensitivity Analysis

The first test investigates the impact of varying the resolution of the transmission graph as defined in Section 3.3. The number of bucket nodes is adjusted for each track, and the train nodes are clustered with a specified maximum clustering distance. For each test configuration, we analyzed 10 instances optimizing different 100 second intervals of the sunday timetable and present the mean value of the results. Table 2 displays the percentage reduction in the number of buckets for different resolutions compared to using one bucket for each departure configuration. The column ∞ indicates that we have exactly one bucket for each track. Additionally, Table 3 presents the relative difference in the objective function values compared to the case with one bucket per train node for the quadratic model CM, its most accu-

Table 2: Percentage of bucket nodes reduced by various resolutions.

Instance	0.05	0.1	0.5	1.0	∞
CM	34.40%	48.04%	72.70%	77.97%	81.49%

rate linearization SB and the relaxed model RLX. The results in Table 2 indicate

Table 3: Relative difference in the objective value to the quadratic model CF for different models and resolutions.

Instance	0.05	0.1	0.5	1.0	∞
CM	0.01%	0.02%	0.04%	0.05%	0.02%
RLX	0.04%	0.29%	2.61%	4.67%	5.92%
SB	0.16%	0.05%	3.01%	2.73%	3.45%

that we can already reduce almost half of the train nodes with a resolution of 0.1. Decreasing the number of buckets in the transmission graph leads to a reduction of bucket nodes by up to 81.49% but also comes with significantly higher deviations from the objective value using one bucket for each train node. This has led us to use a resolution of 0.1 in the following computational tests in relation to the solution strategies.

4.3 Solving Strategy Comparison

The second test compares different solving strategies for instances with 4 different time horizons between 100 and 700 seconds. The strategies include the solving of the models $BASE$, RLX, and SB as well as the different implementations for the developed Benders decomposition approach BS and BCB. Each strategy gets the solution of $BASE$ as a starting solution. For each timetable and time horizon, we solve 5 different timetable segments with a maximum runtime set to 5 hours. Table 4 shows the geometric mean of the resulting runtimes, Table 5 displays the mean of the *real* energy consumptions of the solutions obtained with each strategy, along with the relative improvement (SAV) compared to $BASE$.

It is important to distinguish between the model used for optimization and the model used for evaluation. While each strategy optimizes its respective model (e.g., $BASE$, RLX, etc.), we evaluate all resulting timetables using the same quadratic current model CF to ensure fair comparison. This evaluation model, solved using the heuristic HEU from Section 2.5, represents the most accurate representation of the physical power flows.

For Model $BASE$, we present two values:

- Column $BASE$ shows the real energy consumption (evaluated with CF) of the solution that was optimal according to the simplified $BASE$ model
- Column $BASE^*$ shows the lowest real energy consumption among all solutions encountered during the optimization process of $BASE$, including solutions that were suboptimal for $BASE$

This distinction is important because $BASE$ uses simplified power flow assumptions. Therefore, a solution that is suboptimal according to $BASE$ might actually perform better when evaluated with the more accurate CF model. The evaluation times are not included in Table 4.

Table 4: Runtimes for different solving strategies.

Instance	BASE	RLX	BS	BCB	SB
sunday_100	0.06	158.37	3.19	23.73	5374.34
sunday_300	0.14	2205.56	14.01	98.79	18000
sunday_500	0.21	4148.25	26.90	238.47	18000
sunday_700	0.24	4760.78	17.32	263.90	18000
weekday_100	0.14	1038.48	15.79	76.60	18000
weekday_300	0.70	14659.51	142.58	1295.00	18000
weekday_500	1.25	18000	245.49	3616.97	18000
weekday_700	1.44	18000	77.37	5401.85	18000
Average	0.50	7871.37	67.83	1376.91	16421.79

Table 5: Power provided by the powerstations in Wh for timetables computed with different solving strategies.

Instance	BASE	BASE*	RLX	BS	BCB	SB	SAV
sunday_100	179.74	179.74	179.38	**179.35**	179.36	179.69	0.22%
sunday_300	575.49	575.49	**574.89**	574.94	574.93	575.49	0.10%
sunday_500	955.31	955.21	**954.69**	954.79	954.77	955.29	0.07%
sunday_700	1360.61	1359.89	**1359.20**	1361.88	1359.83	1360.23	0.10%
weekday_100	302.52	302.46	300.14	**300.12**	300.16	302.52	0.79%
weekday_300	1023.30	1020.21	1017.34	**1016.59**	1017.05	1023.30	0.65%
weekday_500	1714.37	1710.92	1702.37	1700.81	**1700.77**	1712.31	0.79%
weekday_700	2415.97	2413.44	**2408.32**	2412.83	2408.36	2415.97	0.32%

The integrated view of schedule and DC power network optimization yields noticable improvements particularly for the weekday timetables, where there are more trains driving simultaneously in the network than on Sundays.

While the simplified $BASE$ model neglects power losses and does not provide the most accurate energy consumption estimates, its short runtime makes it useful for real-time applications. The developed fast simulation heuristic that efficiently evaluates the energy consumption of its output timetables enhances its practicality. It allows us to assess multiple solutions generated during the solving process and select the best one, as done in $BASE^*$.

For non-real-time settings, models that incorporate power losses produce more accurate and reliable solutions. While solving the most detailed model, SB, to optimality was infeasible within a five-hour time limit for most instances, the introduced linearized model and the Benders decomposition approach significantly improved the runtime of RLX. These advancements make the physically accurate model practically applicable for medium-sized timetabling problems.

5 Conclusions

In conclusion, this paper represents a fusion of two critical areas of research: timetable optimization and DC power grid optimization in the context of underground railway systems. By combining these previously disparate fields, we have developed a novel approach for generating energy-efficient timetables that accounts for the intricate dynamics of the power network. Our work extends beyond conventional timetable

optimization by accurately modeling the physical laws and power losses inherent in the DC power grid, thus ensuring a more comprehensive understanding of energy consumption and demand within the railway system.

For real-time applications, we explored a simplified optimization approach that neglects power losses but offers the advantage of extremely short computation times. To enhance its practical usability, we developed a fast simulation heuristic that estimates energy consumption efficiently. This allows multiple solutions generated during the optimization process to be assessed in real time, enabling the selection of the most energy-efficient timetable.

For settings where real-time performance is not required, we introduced a linearized formulation of a detailed model that incorporates power losses and provides more accurate and reliable energy consumption estimates. The developed Benders decomposition approach significantly improved the runtime of the detailed model, which makes the physically accurate energy-consumption model applicable to medium-sized timetabling problems in practice.

Empirical validation using real-world data from the VAG demonstrated the effectiveness of our integrated approach. The simulated energy consumption closely matched actual measurements, with a deviation of at most 1%, confirming the accuracy of our model. Additionally, the optimized timetable achieved an increase in energy efficiency of up to 0.8% compared to the previously used scheduling approach, highlighting the tangible benefits of incorporating power flow dynamics into timetable optimization.

Beyond the immediate improvements in energy efficiency and computational performance, this research contributes to the broader field of railway operations by integrating physical energy dynamics with timetable optimization. The methodologies developed in this work provide a foundation for further research at the intersection of transportation and energy systems, with potential applications in other domains where energy efficiency and operational optimization are critical. As urban centers continue to expand, the demand for sustainable and efficient public transportation will grow, making the contributions of this paper increasingly relevant for the operation of next-generation railway systems.

References

Arboleya, Pablo et al. (2020). "A review of railway feeding infrastructures: Mathematical models for planning and operation". In: *eTransportation* 5, p. 100063. DOI: https://doi.org/10.1016/j.etran.2020.100063.

Bärmann, Andreas et al. (2021). "Energy-Efficient Timetabling in a German Underground System". In: *German Success Stories in Industrial Mathematics*. Cham: Springer International Publishing, pp. 105–112. ISBN: 978-3-030-81455-7. DOI: 10.1007/978-3-030-81455-7_18.

Berriel, Ryan O et al. (2023). "Analysis of the Timetable Impact on Energy Consumption of a Subway Line". In: *IEEE Transactions on Vehicular Technology*. DOI: 10.1109/TVT.2023.3282816.

Eurostat (2024). "Electricity prices for non-household consumers - bi-annual data". In: *Energy Statistics - prices of natural gas and electricity*.

Gan, Lingwen and Steven H Low (2014). "Optimal power flow in direct current networks". In: *IEEE Transactions on Power Systems* 29.6, pp. 2892–2904. DOI: 10.1109/TPWRS.2014.2313514.

Gao, Ziyou and Lixing Yang (2019). "Energy-saving operation approaches for urban rail transit systems". In: *Frontiers of Engineering Management* 6.2, pp. 139–151. DOI: https://doi.org/10.1007/s42524-019-0030-7.

Gemander, Patrick, Andreas Bärmann, and Alexander Martin (2023). "A Stochastic Optimization Approach to Energy-Efficient Underground Timetabling under Uncertain Dwell and Running Times". In: *Transportation Science* 57.6, pp. 1627–1645. DOI: https://doi.org/10.1287/trsc.2022.0269.

Gupta, Shuvomoy Das, Bart PG Van Parys, and J Kevin Tobin (2023). "Energy-optimal Timetable Design for Sustainable Metro Railway Networks". In: *arXiv preprint arXiv:2309.05489*. DOI: https://doi.org/10.48550/arXiv.2309.05489.

Hager, Lukas and Tobias Kuen (2024). "Optimization of Underground Train Systems". en. In: *Unlocking Artificial Intelligence: From Theory to Applications*. Ed. by Christopher Mutschler et al. Cham: Springer Nature Switzerland, pp. 303–319. ISBN: 978-3-031-64832-8. DOI: https://doi.org/10.1007/978-3-031-64832-8.

Huang, Kang, Feixiong Liao, and Ziyou Gao (2021). "An integrated model of energy-efficient timetabling of the urban rail transit system with multiple interconnected lines". In: *Transportation Research Part C: Emerging Technologies* 129, p. 103171. DOI: https://doi.org/10.1016/j.trc.2021.103171.

Kang, Liujiang et al. (2024). "A Critical Review of Subway Train Timetabling and Rescheduling Problems". In: *IEEE Transactions on Intelligent Transportation Systems*. DOI: 10.1109/TITS.2024.3386728.

Liu, Hongjie et al. (2018). "Timetable optimization for regenerative energy utilization in subway systems". In: *IEEE Transactions on Intelligent Transportation Systems* 20.9, pp. 3247–3257. DOI: 10.1109/TITS.2018.2873145.

Liu, Pei et al. (2018). "Energy-efficient train timetable optimization in the subway system with energy storage devices". In: *IEEE Transactions on Intelligent Transportation Systems* 19.12, pp. 3947–3963. DOI: 10.1109/TITS.2018.2789910.

Moreno, Teresa et al. (2015). "Urban air quality comparison for bus, tram, subway and pedestrian commutes in Barcelona". In: *Environmental Research* 142, pp. 495–510. DOI: https://doi.org/10.1016/j.envres.2015.07.022.

Peña-Alcaraz, Maite et al. (2012). "Optimal underground timetable design based on power flow for maximizing the use of regenerative-braking energy". In: *Proceedings of the Institution of Mechanical Engineers, Part F: Journal of Rail and Rapid Transit* 226.4, pp. 397–408. DOI: https://doi.org/10.1177/0954409711429411.

Raghunathan, A. U. et al. (2014). "Minimizing Energy Consumption In Railways By Voltage Control On Substations". In: *WIT Transactions on The Built Environment* 135, pp. 697–708. DOI: https://doi.org/10.2495/CR140581.

Scheepmaker, Gerben M, Rob MP Goverde, and Leo G Kroon (2017). "Review of energy-efficient train control and timetabling". In: *European Journal of Operational Research* 257.2, pp. 355–376. DOI: https://doi.org/10.1016/j.ejor.2016.09.044.

Su, Shuai et al. (2013). "A subway train timetable optimization approach based on energy-efficient operation strategy". In: *IEEE transactions on intelligent transportation systems* 14.2, pp. 883–893. DOI: 10.1109/TITS.2013.2244885.

Thomas, Llewellyn H (1949). "Elliptic problems in linear differential equations over a network". In: *Watson Scientific Computing Laboratory Report* 1.

Verkehrsgesellschaft Frankfurt am Main (VGF) (2022). *Nachhaltigkeitsbericht 2022*. Frankfurt am Main.

Yang, Songpo et al. (2020). "A bi-objective timetable optimization model incorporating energy allocation and passenger assignment in an energy-regenerative metro system". In: *Transportation Research Part B: Methodological* 133, pp. 85–113. DOI: https://doi.org/10.1016/j.trb.2020.01.001.

Yang, Xin et al. (2015). "An energy-efficient scheduling approach to improve the utilization of regenerative energy for metro systems". In: *Transportation Research Part C: Emerging Technologies* 57, pp. 13–29. DOI: https://doi.org/10.1016/j.trc.2015.05.002.

Zhao, Ning et al. (2017). "An integrated metro operation optimization to minimize energy consumption". In: *Transportation Research Part C: Emerging Technologies* 75, pp. 168–182. DOI: 10.1109/TITS.2018.2871347.

Zhou, Yuhe et al. (2018). "Integrated optimization on train control and timetable to minimize net energy consumption of metro lines". In: *Journal of Advanced Transportation* 2018.1, p. 7905820. DOI: https://doi.org/10.1155/2018/7905820.